Heliyon 9 (2023) e13091

Contents lists available at ScienceDirect

Heliyon

journal homepage: www.cell.com/heliyon

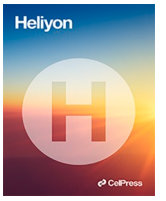

Research article

Scrutinization of second law analysis and viscous dissipation on Reiner-RivlinNanofluid with the effect of bioconvection over a rotating disk

Farhan Ali [a], A. Zaib [a], K. Loganathan [b], Anwar Saeed [c], Thidaporn Seangwattana [d,*], Poom Kumam [c,e,**], Ahmed M. Galal [f,g]

[a] Department of Mathematical Sciences, Federal Urdu University of Arts, Sciences & Technology, Gulshan-e-Iqbal Karachi, 75300, Pakistan
[b] Department of Mathematics and Statistics, Manipal University Jaipur, Jaipur, 303007, Rajasthan, India
[c] Center of Excellence in Theoretical and Computational Science (TaCS-CoE), Faculty of Science, King Mongkut's University of Technology Thonburi (KMUTT), 126 PrachaUthit Rd., Bang Mod, ThungKhru, Bangkok, 10140, Thailand
[d] Faculty of Science Energy and Environment, King Mongkut's University of Technology North Bangkok, Rayong Campus (KMUTNB), 21120, Rayong, Thailand
[e] Department of Medical Research, China Medical University Hospital, China Medical University, Taichung, 40402, Taiwan
[f] Department of Mechanical Engineering, College of Engineering in Wadi Alddawasir, Prince Sattam bin Abdulaziz University, Saudi Arabia
[g] Production Engineering and Mechanical Design Department, Faculty of Engineering, Mansoura University, P.O 35516, Mansoura, Egypt

ARTICLE INFO

Keywords:
MHD
Reiner-Rivlin
Viscous dissipation
Thermal radiation

ABSTRACT

In comparison to Newtonian fluids, non-Newtonian fluids have fascinating features in heat transportation. Here, newly type of Reiner-Rivlinnanoliquid flow over the revolving disk for viscous dissipation (VD) is being explored in a multiple-slip effect. The inclusion of gyrotactic microorganisms in the nanoliquid enhances the tendency of the nanoparticles. The idea of the intended model is enhanced by considering in the impact of activation energy, thermal radiative, heated convective conditions and entropy minimization. The system of nonlinear PDE is constructed into nonlinear ODE's by applying the von-Karman similarity method and later solved numerically using the BVP4c solver which is considered to study the complicated ordinary differential equations. TheInfluence of various parameters is elaborated and plotted physically through the graphical illustration. By contrasting the reported data in the restricted form to a previously published article, the accuracy of the current model has examined. The impact of a non-Newtonian fluid parameter over the velocity field appeared to showdpreciation in it. The results elucidate that when the wall slip coefficient is larger more torque is needed to maintain constant disk revaluation. Surface heat transmission and wall skin friction are computed for a wide variety of factors. These flows have several real world-applications, including modeling cases that occur in oceanography and geophysics, various industrial fields (such as lumber production).

* Corresponding author.
** Corresponding author. Center of Excellence in Theoretical and Computational Science (TaCS-CoE), Faculty of Science, King Mongkut's University of Technology Thonburi (KMUTT), 126 PrachaUthit Rd., Bang Mod, ThungKhru, Bangkok, 10140, Thailand.
E-mail addresses: thidaporn.s@sciee.kmutnb.ac.th (T. Seangwattana), poom.kum@kmutt.ac.th (P. Kumam).

https://doi.org/10.1016/j.heliyon.2023.e13091
Received 5 September 2022; Received in revised form 10 January 2023; Accepted 17 January 2023
Available online 20 January 2023

1. Introduction

In the modern era, nanofluids have producedenormousconsideration due to their noteworthy thermal transport and fascinating features in several fields, such as computer processes, hybrid power, fuel cell, and other high-energy devices. Nanoliquid has high thermal conductivity and better constancy that avert fast settling. For the increment of thermal conductivity, scholars scrutinized it theoretically and experimentally. Choi [1] proposed the term nanofluid. Later, Tiwari and Das [2] and Buongiorno [3] presented the two distinct nanofluid models with thermal properties. Khan et al. [4] described a 3D flow of nanofluid with convective conditions past an extending sheet. Mansur and Ishak [5] examined 3D nanoliquidpastan extending sheet. Sheiholeslami and co-worker [6]. narrated the MHD nanoparticles with heat transfer. Alghamdi [7] analyzed the features of MHD mixed convection flow of nano-materialduetoaspinning disk with activation energy and chemical reaction. The effect on the time-dependent 3-D spinning Flow of SWCN along nonlinear thermal radiativeas viscous dissipation wasexaminedbyJawad et al. [8]. Shah and co-workers [9]investigated the thin film flow through MHD nanofluidpast a horizontally revolving disk with the effect of nonlinear thermal radiation. Recently, the slip effect of Reiner-Rivlinnanoparticlesin pasta revolvingdiskshas been investigated numerically by Naqvi et al. [10]. More about the significance of nanofluid can be observed in Refs. [11–14].

Fluid flow and heat transfer are fascinating due to revolving disks and play a remarkable role in various technical applications such as rotor statorsandelectronic and rotary devices. The pinioning work has been proposed by Von-Karman [15],whoconsidered that a disk of more significant radial velocity rotates with fixed rotationalspeed. The fluid closes to the disk in a radial direction owing to the weak Influence of centrifugal force. This fluid via a descending spiraling movement is mentioned chiefly because of the free disk pumping effect. Many scholars have investigated this arena to show the new finding on rotating disks with fluid. The asymptotic solutions are given by Cohran [16] to the accurate solution of Von-Kraman. The heat transfer analysis with several Prandtl numbers for Von-Karman is probed by Millsaps and Pholhalusen [17]. Ackroyd [18] assumed suction occurrence over a permeable rotating disk with an exponentially decaying function. Batchelor [19] studied the particular case of Von-Karman,resultinginsome angular velocities about the same axis in the disk and ambient fluid. One more point where the fluid at infinity is rotating as the disk is fixed state has been examined by Bodewadt [20]. ZandbergenandDijkstra [21] proposed a complete review of the literature related to rotating disks. The swirling flow of viscoelastic fluid over a rotating disk with a series approximation solution is inspected by Ariel [22]. Miclavcic and Wang [23] addressed the slip flow numerically over rotating disks for a broader variety of slip coefficients. Chawla et al. [24] presented a special case of the Von-Karman problem in which disk and fluid are both at infinity concerningasimilar axis. Turkyilmazoglu [25] modelled the effect of a magnetic field over stretched rotating disk near the stagnation point. Many researchers have examined various flow configurations comprising the rotating fluid [26–35].

The term “non-Newtonian fluid” refers to a specific category of fluids that have different technological and industrial applications than “Newtonian” fluids. In nature, many models of non-Newtonian have been presented over time. The current examination considers the simplest model, namely the Reiner-Rivlin fluid model. The model was coined by Reiner [36] and Rivlin [37]. This model explains the geological production, chemical, and biological process and is crucial in dynamic rotating disk systems. A problem formulation of viscoelastic fluid past a rotating disk with a perturbation solution is explained by Elliot [38]. The viscoelastic flow over a rotating disk has been designed by Ariel [39]. The self-similar solution of the power-law model has been developed through Von-Karman flow by Andersson and Korte [40]. Osalusi et al. [41] examined the visco-plastic fluid on Bingham. Attia [42] established the Reiner-Rivlin fluid due to the revolving disk in an inelastic fluid. Afterwards, a similar model was investigated by Sahoo [43]. He implemented the partial slip conditions. The Bingham liquids due to rotating disks have been presented by Ahmadpour and Sadeghy [44]. They computed with an accurate numerical solution on MATLAB bvpc4. The effects of heat generation/absorption and second-grade fluid over rotating disks with homogenous-heterogamous reactions have been reported by Imtiaz [45]. A more recent, asymptotic numerical

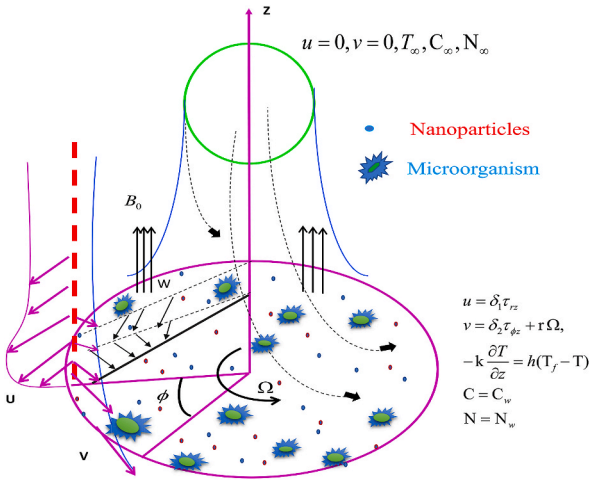

Fig. 1. Geometry of the problem.

solution Reiner-Rivlin fluid and Bodewadt flow over the stretching surface are arranged by Shaoo and Shevchuk [46]. Most Recently, Pei et al. [47] discussed the combined effect of Cattaneo-Cristove heat flux with Bioconvection flow for Reiner-Rivlinnanofluiddue to a revolving disk.

It has been brought to our attention in the primary research that the most recent flow model has not been investigated as of yet. We examine the activation energy with a gyrotactic microorganism of the Reiner-Rivlin fluid due to revolving disks comprising nanoparticles. The Constitutive boundary conditions are also encountered. The current problem is developed with the help of the BVP4c technique. Nanoparticles induce the thermophoretic and Brownian motion phenomena. Plots are used to analyze the distribution profiles for velocity, temperature, concentration, and motile density tablesfor skin friction, Nusselt number, Sherwood number, and motile microorganisms.

2. Physical problem and model formulation

Here non-transient, incompressible bio-convection flow of Reiner-Rivlinnanofluid through a spinning disc with various slip conditions is examined. The disk is rotating rigidly along its vertical axis at a constant angular speed Ω, creating a swirling flow in the nearby fluid layers as seen in Fig. 1.The velocitycomponentsare u, v and w respectively, in the directions of r, φ and z. Due to axial symmetry, the azimuthally coordinate u is independent of the velocity components. The boundary layer thickness is assumed to be greater than the typical scale of the protuberance, and conditions for velocityslipare then applied. The relationship described below is created by Reiner and Rivlin [36,37], and also by Raza et al. [47] are given in Eq. (1) to Eq. (5).

The Reiner-Rivlin in the form of the stress tensor is given as:

$$\tau_{ij} = -p\delta_{ij} + \mu e_{ij} + \mu_c e_{ik} e_{kj}; e_{jj} \tag{1}$$

Here, $e_{ij} = \left(\frac{\partial u_i}{\partial x_j}\right) + \left(\frac{\partial u_j}{\partial x_i}\right)$, δ_{ij}, μ, μ_c, p, and e_{jj} is represented by the Kronecker delta, the dynamic viscosity of coefficient, cross-viscosity coefficient, pressure and deformation rate tensor.

The following governing equations can be expressed as

$$\frac{\partial u}{\partial r} + \frac{u}{r} + \frac{\partial w}{\partial z} = 0 \tag{2}$$

$$\rho\left(u\frac{\partial u}{\partial r} - \frac{v^2}{r} + w\frac{\partial w}{\partial z}\right) = \frac{\partial \tau_{rr}}{\partial r} + \frac{\partial \tau_{rz}}{\partial z} + \frac{\tau_{rr} - \tau_{\varphi\varphi}}{r} - \sigma B_0^2 u \tag{3}$$

$$\rho\left(u\frac{\partial u}{\partial r} + \frac{uv}{r} + w\frac{\partial v}{\partial z}\right) = \frac{1}{r^2}\frac{\partial}{\partial r}\left(\mathrm{r}^2\tau_{r\varphi}\right) + \frac{\partial \tau_{r\varphi}}{\partial z} + \frac{\tau_{r\varphi} - \tau_{\varphi r}}{r} - \sigma {B_0}^2 v \tag{4}$$

$$\rho\left(u\frac{\partial w}{\partial r} + w\frac{\partial w}{\partial z}\right) = \frac{1}{r}\frac{\partial}{\partial r}(\mathrm{r}\tau_{rz}) + \frac{\partial \tau_{zz}}{\partial z} \tag{5}$$

The deformation of the stress tensor is defined as [37].

$$\begin{aligned} &e_{rr} = 2\frac{\partial u}{\partial r}, e_{\varphi\varphi} = 2\frac{u}{r}, e_{zz} = 2\frac{\partial w}{\partial z}, e_{r\varphi} = e_{\varphi r} = r\frac{\partial}{\partial r}\left(\frac{v}{r}\right), \\ &e_{z\varphi} = e_{\varphi z} = \frac{\partial v}{\partial r}, e_{zr} = e_{zr} = \frac{\partial u}{\partial z} + \frac{\partial w}{\partial r}, \end{aligned} \tag{6}$$

Stress tensor components [48] are considered as Eq. (7) to Eq. (12)

$$\tau_{rr} = -p + \mu 2\left(\frac{\partial u}{\partial r}\right) + \mu_c\left[4\left(\frac{\partial u}{\partial r}\right)^2 + \left(\frac{\partial u}{\partial r} + \frac{\partial w}{\partial r}\right)^2 + \left(\frac{\partial v}{\partial r} - \frac{v}{r}\right)^2\right], \tag{7}$$

$$\tau_{zr} = \mu\left(\frac{\partial u}{\partial z} + \frac{\partial w}{\partial r}\right) + \mu_c\left[\begin{array}{l}\left(\frac{\partial u}{\partial z} + \frac{\partial w}{\partial r}\right)^2\left(2\frac{\partial u}{\partial r}\right) + \left(\frac{\partial v}{\partial z}\right)\left(\frac{\partial v}{\partial r} - \frac{\partial v}{\partial r}\right) \\ + \left(2\frac{\partial w}{\partial z}\right)\left(\frac{\partial u}{\partial z} + \frac{\partial w}{\partial r}\right)\end{array}\right], \tag{8}$$

$$\tau_{\varphi\varphi} = -p + \mu\left(2\frac{u}{r}\right) + \mu_c\left[4\left(\frac{u}{r}\right)^2 + \left(\frac{\partial v}{\partial z}\right)^2 + \left(\frac{\partial v}{\partial r} - \frac{v}{r}\right)^2\right], \tag{9}$$

$$\tau_{zr} = \mu\left(\frac{\partial u}{\partial z} + \frac{\partial w}{\partial r}\right) + \mu_c\left[\begin{array}{l}\left(\frac{\partial u}{\partial z} + \frac{\partial w}{\partial r}\right)^2\left(2\frac{\partial u}{\partial r}\right) + \left(\frac{\partial v}{\partial z}\right)\left(\frac{\partial v}{\partial r} - \frac{\partial v}{\partial r}\right) \\ + \left(2\frac{\partial w}{\partial z}\right)\left(\frac{\partial u}{\partial z} + \frac{\partial w}{\partial r}\right)\end{array}\right], \tag{10}$$

$$\tau_{r\varphi}=\mu\left(\frac{\partial v}{\partial r}-\frac{v}{r}\right)+\mu_c\left[\left(\frac{\partial v}{\partial r}-\frac{v}{r}\right)^2\left(2\frac{\partial u}{\partial r}\right)+\left(\frac{2u}{r}\right)\left(\frac{\partial v}{\partial r}-\frac{v}{r}\right)+\left(\frac{\partial v}{\partial z}\right)\left(\frac{\partial u}{\partial z}+\frac{\partial w}{\partial r}\right)\right], \tag{11}$$

$$\tau_{z\varphi}=\mu\left(\frac{\partial v}{\partial z}\right)+\mu_c\left[\left(\frac{\partial u}{\partial z}+\frac{\partial w}{\partial r}\right)^2\left(\frac{\partial v}{\partial r}-\frac{v}{r}\right)+2\left(\frac{\partial v}{\partial z}\left(\frac{u}{r}\right)+\frac{\partial w}{\partial z}\frac{\partial v}{\partial z}\right)\right], \tag{12}$$

$$\tau_{zz}=-p+2\mu\left(\frac{\partial w}{\partial z}\right)+\mu_c\left[4\left(\frac{\partial w}{\partial z}\right)^2+\left(\frac{\partial v}{\partial z}\right)^2+\left(\frac{\partial u}{\partial z}+\frac{\partial w}{\partial r}\right)^2\right], \tag{13}$$

Using Eqs. (3)–(5)

$$u\frac{\partial u}{\partial r}-\frac{v^2}{r}+w\frac{\partial u}{\partial z}=\nu\frac{\partial^2 u}{\partial z^2}+\frac{\mu_c}{\rho}\begin{pmatrix}4\frac{\partial u}{\partial z}\frac{\partial^2 u}{\partial r\partial z}+2\frac{\partial u}{\partial r}\frac{\partial^2 u}{\partial z^2}+2\frac{\partial w}{\partial z}\frac{\partial^2 u}{\partial z^2}+\\ \frac{\partial^2 v}{\partial z^2}\left(\frac{\partial v}{\partial z}-\frac{v}{r}\right)+\frac{\partial v}{\partial z}\left(\frac{\partial^2 v}{\partial z\partial r}-\frac{1}{r}\frac{\partial v}{\partial z}\right)\\ +2\frac{\partial u}{\partial z}\frac{\partial^2 w}{\partial z^2}+\frac{1}{r}\left(\left(\frac{\partial u}{\partial z}\right)^2-\left(\frac{\partial v}{\partial z}\right)^2\right)\end{pmatrix}-\frac{\sigma {B_0}^2}{\rho}u \tag{14}$$

$$u\frac{\partial v}{\partial r}+\frac{uv}{r}+w\frac{\partial v}{\partial z}=\nu\frac{\partial^2 v}{\partial z^2}+\frac{\mu_c}{\rho}\begin{pmatrix}\frac{\partial v}{\partial z}\frac{\partial^2 u}{\partial z\partial r}+\frac{\partial u}{\partial z}\frac{\partial^2 v}{\partial z\partial r}+\frac{4}{r}\frac{\partial u}{\partial z}\frac{\partial v}{\partial z}\\ \frac{\partial^2 u}{\partial z^2}\left(\frac{\partial v}{\partial z}-\frac{v}{r}\right)+\frac{\partial u}{\partial z}\left(\frac{\partial^2 v}{\partial z\partial r}-\frac{1}{r}\frac{\partial v}{\partial z}\right)\\ +2\frac{\partial w}{\partial z}\frac{\partial^2 v}{\partial z^2}+2\frac{\partial v}{\partial z}\frac{\partial^2 w}{\partial z^2}\end{pmatrix}-\frac{\sigma {B_0}^2}{\rho}v \tag{15}$$

$$\begin{aligned}u\frac{\partial T}{\partial r}+w\frac{\partial T}{\partial z}=\alpha\frac{\partial^2 T}{\partial z^2}+\tau\left[D_B\frac{\partial C}{\partial z}\frac{\partial T}{\partial z}+\frac{D_T}{T_\infty}\left(\frac{\partial T}{\partial z}\right)^2\right]\\ -\frac{1}{\rho c_p}\frac{\partial q_r}{\partial z}+\frac{\mu}{\rho c_p}\left(\left[\frac{\partial u}{\partial z}\right]^2+\left[\frac{\partial v}{\partial z}\right]^2\right)\end{aligned} \tag{16}$$

$$u\frac{\partial C}{\partial r}+w\frac{\partial C}{\partial z}=D_B\frac{\partial^2 C}{\partial z^2}+\frac{D_T}{T_\infty}\frac{\partial^2 T}{\partial z^2}-K_r^2\left(\frac{T}{T_\infty}\right)^n\exp\left(\frac{E_0}{\kappa T}\right)(C-C_\infty) \tag{17}$$

$$u\frac{\partial N}{\partial r}+w\frac{\partial N}{\partial z}=-\frac{bW_c}{(C_w-C_\infty)}\left[\frac{\partial}{\partial z}\left(N\frac{\partial C}{\partial z}\right)\right]+D_N\frac{\partial^2 N}{\partial z^2} \tag{18}$$

Boundary conditions [37]are considered in Eq. (19)

$$\left.\begin{aligned}&u=\delta_1\tau_{zr},v=\delta_2\tau_{z\varphi}+r\Omega,w=0,-k\frac{\partial T}{\partial z}=h\left(T_f-T\right),C=C_w,\\ &N=N_w=0\ \ at\ z=0,\\ &u\ \to 0,v\to 0,w\to 0,T\to T_\infty,C\to C_\infty,\Upsilon\to\Upsilon_\infty\ at\ z\to\infty.\end{aligned}\right\} \tag{19}$$

Here, T is the temperature, C is the concentration, N is the motile density of the fluid, ρ denotes the density of the fluid, k denotes the thermal conductivity, α_m thermal diffusivity, $(\rho c)_p$ nanoparticles tendency, $(\rho c)_f$ base fluid tendency, T_w, C_w, N_w signify the temperature, the concentration of nanoparticles and motile microorganism, respectively, $T_\infty, C_\infty, N_\infty$ ambient temperature, nanoparticles concentration and motile microorganism, D_B Brownian diffusivity, D_T thermal diffusivity,

The system of Eq. (2) to Eq. (5) and Eq. (14) to Eq. (18) along boundary condition Eq. (19) are turned into ODEs by using the following similarity transformations

$$\left.\begin{aligned}&\xi=\sqrt{\frac{\Omega}{\upsilon}}z,u=r\Omega F^{'},v=r\Omega G,w=-2\sqrt{\Omega\upsilon}F,\mu\Omega P(\xi)=P-P_\infty,\\ &\theta(\xi)=\frac{T-T_\infty}{T_w-T_\infty},\varphi(\xi)=\frac{C-C_\infty}{C_w-C_\infty},\Upsilon(\xi)=\frac{N-N_\infty}{N_w-N_\infty}.\end{aligned}\right\} \tag{20}$$

Here, ξ is the dimensionless variable, by using above transformations Eq. (20) equations 14–18 reduces to

$$F'''+\lambda\left(F''2-G'2-2F'F'''\right)-F'2+G^2+2FF''-MF'=0 \tag{21}$$

$$G''-2F'G+2FG'+2\lambda(F''G'-F'G'')-MG=0 \tag{22}$$

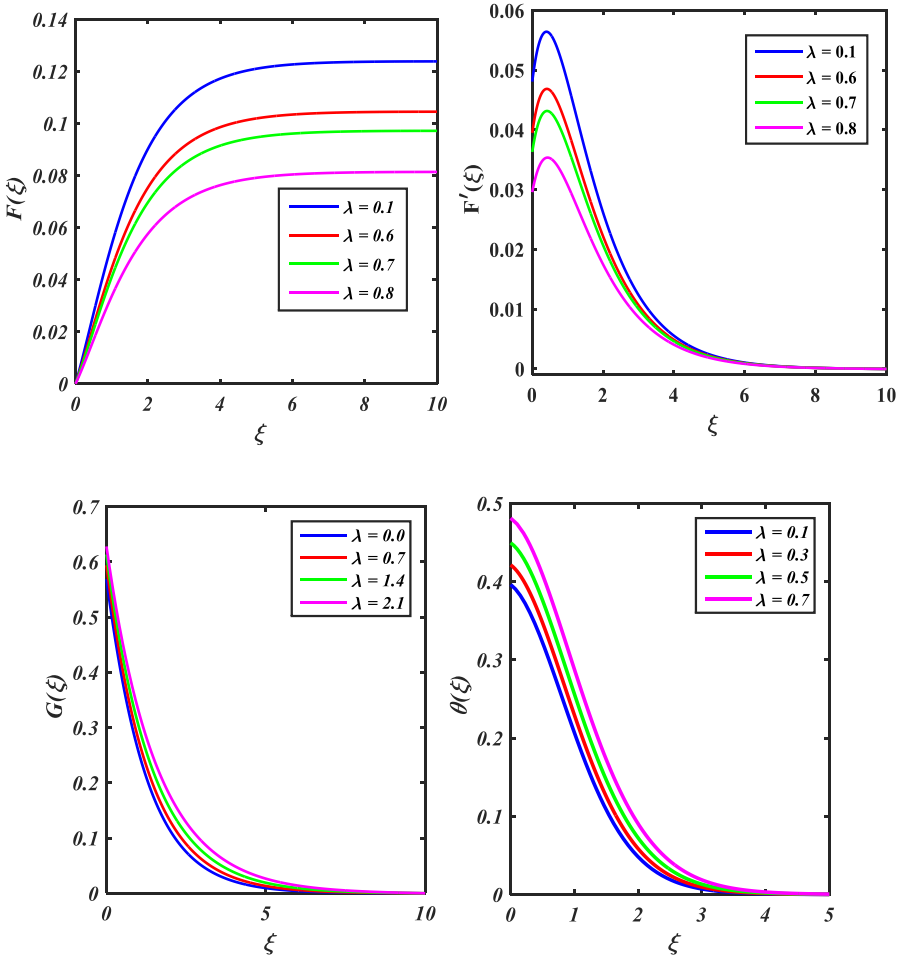

Fig. 2(a–d). Influence of λ (a) $F(\xi)$ (b) $F^{'}(\xi)$ (c)G(ξ) (d) $\theta(\xi)$.

$$\left(1+\frac{4}{3}Rd\right)\theta''+2\,\mathrm{Pr}\,F\theta'+\mathrm{Pr}\left(Nb\theta'\varphi'+Nt\theta'2\right)+Ec\,\mathrm{Pr}\left(F^{'}2+G'2\right)=0 \tag{23}$$

$$\varphi''+2ScF\varphi'+\frac{Nt}{Nb}\theta''-Sc\,\kappa(1+\gamma\theta)^{n}\exp\left(\frac{-E_a}{1+\gamma\theta}\right)\varphi=0 \tag{24}$$

$$\Upsilon''+2LbF\Upsilon'-\mathrm{Pe}[\varphi''(\Upsilon+\omega)+\Upsilon'\varphi']=0 \tag{25}$$

The converted boundary conditions are

$$\left.\begin{array}{l} F(0)=0,F'(0)=\beta_1F''(0)[1-2\lambda F^{'}(0)],G(0)=\beta_2G'(0)[1-2\lambda F^{'}(0)]+1,\\ \theta'(0)=-Bi(1-\theta(0)),\varphi'(0)=1,\Upsilon'(0)=1,\text{at }\xi=0.\\ F^{'}\ \to 0,G\ \to 0,\theta\to 0,\varphi\to 0,\Upsilon\to 0\quad \text{as}\quad \xi\ \to\infty \end{array}\right\} \tag{26}$$

where λ signifies the Reiner-Rivlin fluid parameter, β_1 the radial slip, M themagnetic parameter, Rd the thermal radiation, β_2 the azimuthal slip, Bi the Biot number, E_a the activation energy, Ec the Ekert number, Nb Brownian motion, Nt thermophoretic parameter and Pr the Prandtl number, Sc the Scimdth number, ω the microorganism difference parameter, Lb the bio connection Lewis number, Pe thePeclet number.

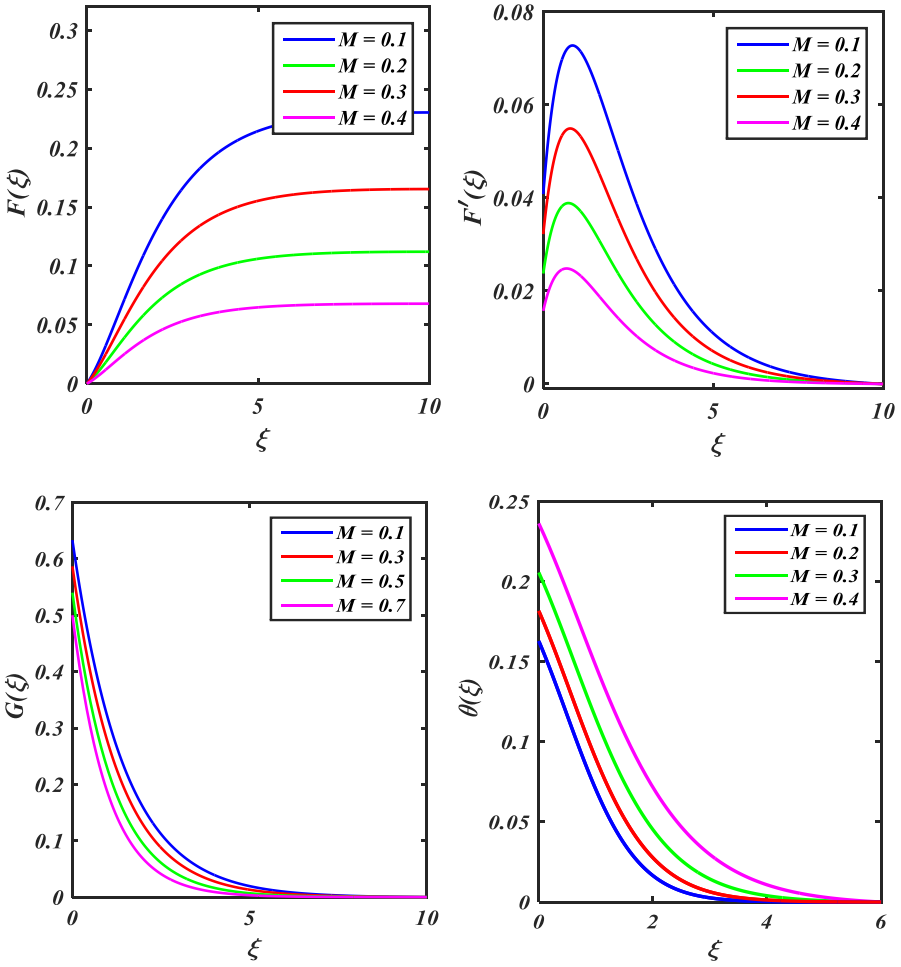

Fig. 3(a–d). Influence of M (a) $F(\xi)$ (b) $F^{'}(\xi)$ (c)G(ξ) (d) $\theta(\xi)$.

$$\lambda=\left(\frac{\mu_c\Omega}{\mu}\right),\beta_1=\left(\rho\sqrt{\Omega\nu}\,\delta_1\right),M=\left(\frac{\sigma B_0^2}{\rho a}\right),\beta_2=\left(\rho\sqrt{\Omega\nu}\,\delta_2\right),Rd=\left(\frac{16\sigma*T_\infty^3}{3k*\nu\rho_{cp}k_0}\right),Bi=\frac{h_f}{k}\left(\sqrt{\frac{\nu_f}{\Omega}}\right),E_a=\left(\frac{E_0}{kT_\infty}\right),$$
$$Ec=\left(\frac{\Omega^2}{bc_p}\right),Nb=\left(\frac{(\rho c_p)_p D_B(C_w-C_\infty)}{(\rho c_p)_f\nu_f}\right),Nt=\left(\frac{(\rho c_p)_p D_T(T_w-T_\infty)}{(\rho c_p)_f T_\infty\nu_f}\right),\Pr=\left(\frac{\mu c_p}{k}\right),Sc=\left(\frac{\nu}{D_B}\right),\omega=\left(\frac{N_\infty}{N_w-N_\infty}\right),$$
$$Lb=\left(\frac{\nu}{D_N}\right),\text{ and }Pe=\left(\frac{bWc}{\nu}\right)$$

2.1. Quantity of engineering importance

$C_{m,r}$ represents the coefficient of moment [47]to measure the least amountoftorque needed is considered in Eq. (27)

$$C_{m,r}=\frac{T_r}{\rho\Omega^2 r^5} \tag{27}$$

where T_r denotes the torque to keep the disk in uniform motion, and is defined as

$$T_r=-\int_0^r \tau_{z\varphi}|_{z=0}2\pi r^2 dr=-\frac{\pi}{2}\rho\Omega\sqrt{\nu\Omega}r^4 G^{'}(0). \tag{28}$$

The physical quantities of C_f, Nu, Sh and Nh is given as

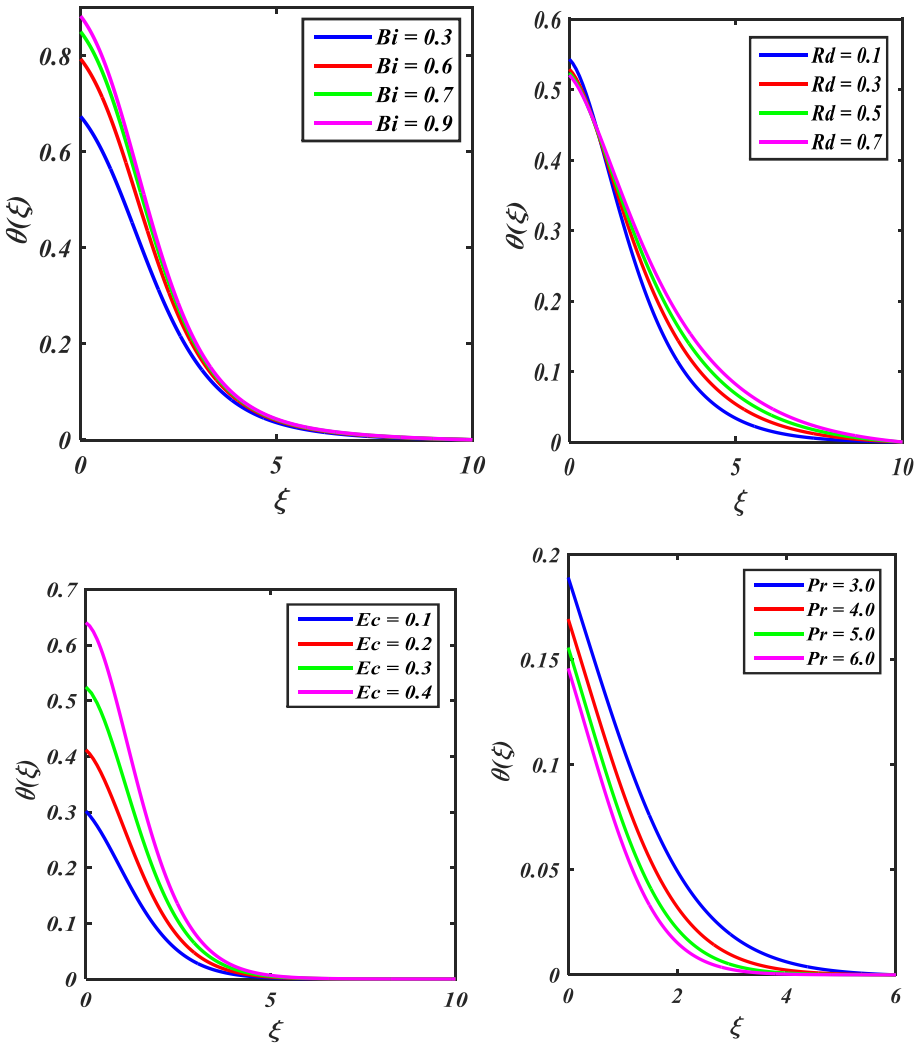

Fig. 4. (a–d) Influence of $\theta(\xi)$ variation in (a) *Bi* (b) *Rd* (c) *Ec* (d) Pr

$$C_f = \frac{\sqrt{\tau_r^2 - \tau_\varphi^2}}{\rho(\mathrm{r}\Omega)^2}, Nu = \frac{rq_w}{k(T_w - T_\infty)}, Sh = \frac{rj_w}{D_B(C_w - C_\infty)}, Nh = \frac{rj_n}{D_N(N_w - N_\infty)} \tag{29}$$

Applying the similarity transformation in Eq. (19), Eq. (28) becomes

$$\left.\begin{aligned} C_f\left(\frac{\Omega r^2}{v}\right)^{1/2} &= \sqrt{(F''(0))^2 + (\mathrm{G}'(0))^2}, Nu\left(\frac{\Omega r^2}{v}\right)^{-1/2}(1+Rd)\theta'(0), \\ Sh\left(\frac{\Omega r^2}{v}\right)^{-1/2} &= \varphi'(0), Nh\left(\frac{\Omega r^2}{v}\right)^{-1/2} = \Upsilon'(0) \end{aligned}\right\} \tag{30}$$

3. Solution methodology

The systemsof Eqs. 21–25constitute the boundary conditions (26), which do not have an analytic solution. Thus, BVP4c technique is considered to obtain the numerical solution. The imitationisestablished to furnishthe solution tothe above nonlinear problem. In the initialstage, converttheqiven system of nonlinear ODEs into first-order ODEs.For the entire mechanism, set new variables as follows:

$$F = P_1, F' = P_2, F'' = P_3, G = P_4, G' = P_5,$$
$$\theta = P_6, \theta' = P_7, \varphi = P_8, \varphi' = P_9, \Upsilon = P_{10}, \Upsilon' = P_{11}$$

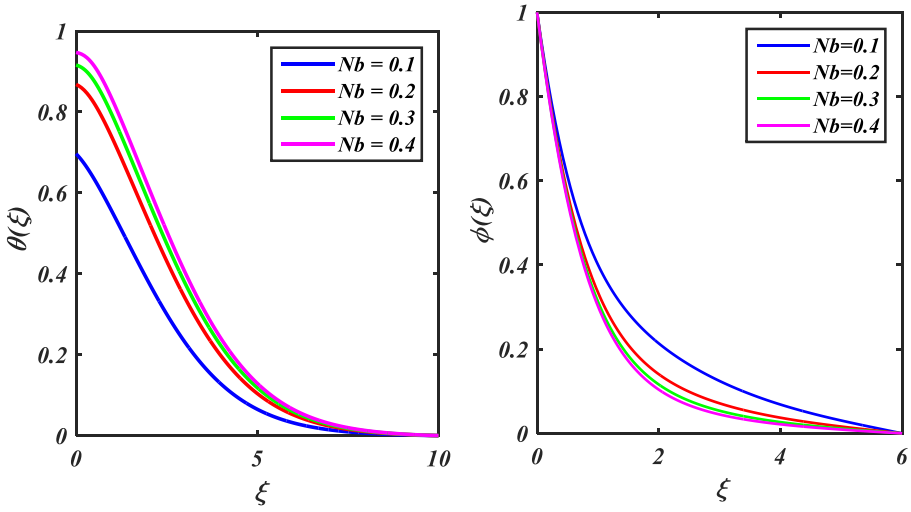

Fig. 5(a–b). Influence of Nb on (a) $\theta(\xi)$ (b) (ξ) .

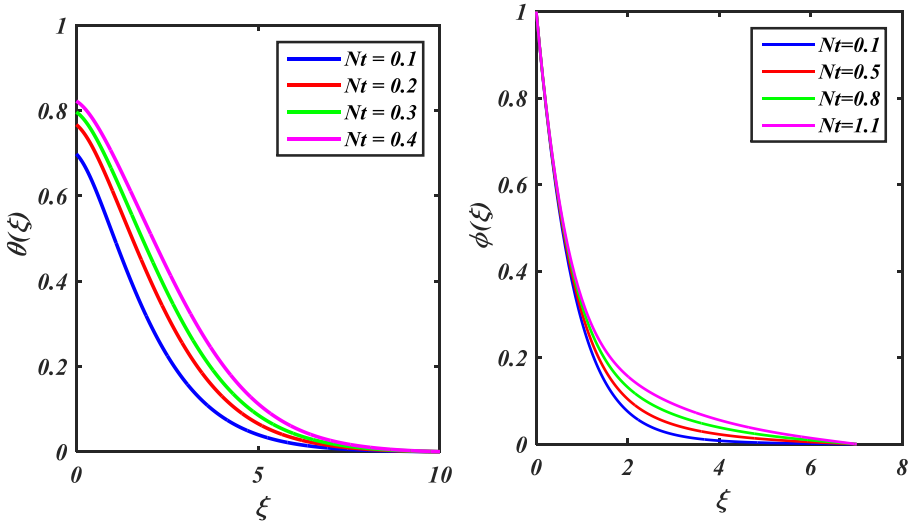

Fig. 6(a–b). Influence of Nt on (a) $\theta(\xi)$ (b) (ξ) .

$$P_3^{'} = \frac{\left(\lambda P_5^2 - \lambda P_3^2 + P_2^2 - P_4^2 - 2P_1P_3 + MP_1\right)}{(1 - 2\lambda P_2)} \tag{31}$$

$$P_5^{'} = \frac{(2P_2P_4 - 2\lambda P_3P_5 - 2P_1P_5 + MP_4)}{(1 - 2\lambda P_2)} \tag{32}$$

$$P_7^{'} = \frac{\left(-2\,\mathrm{Pr}\,P_1P_7 - \mathrm{Pr}\left(NbP_7P_9 + NtP_6^2\right) - Ec\,\mathrm{Pr}\left(P_3^2 + P_5^2\right)(1 - 3KP_2)\right)}{(1 + Rd)} \tag{33}$$

$$P_9^{'} = \left(ScCh(1 + \delta P_6)^n \exp\left[\frac{-E_a}{1 + \delta P_6}\right]P_8 - 2ScP_1P_8 - \frac{Nt}{Nb}P_7^{'}\right) \tag{34}$$

$$P_{11}^{'} = -2LbP_1P_{11} - Pe\left[P_9^{'}(P_{10} + \omega) + P_{11}P_9\right] \tag{35}$$

Subsequently, boundary conditions are

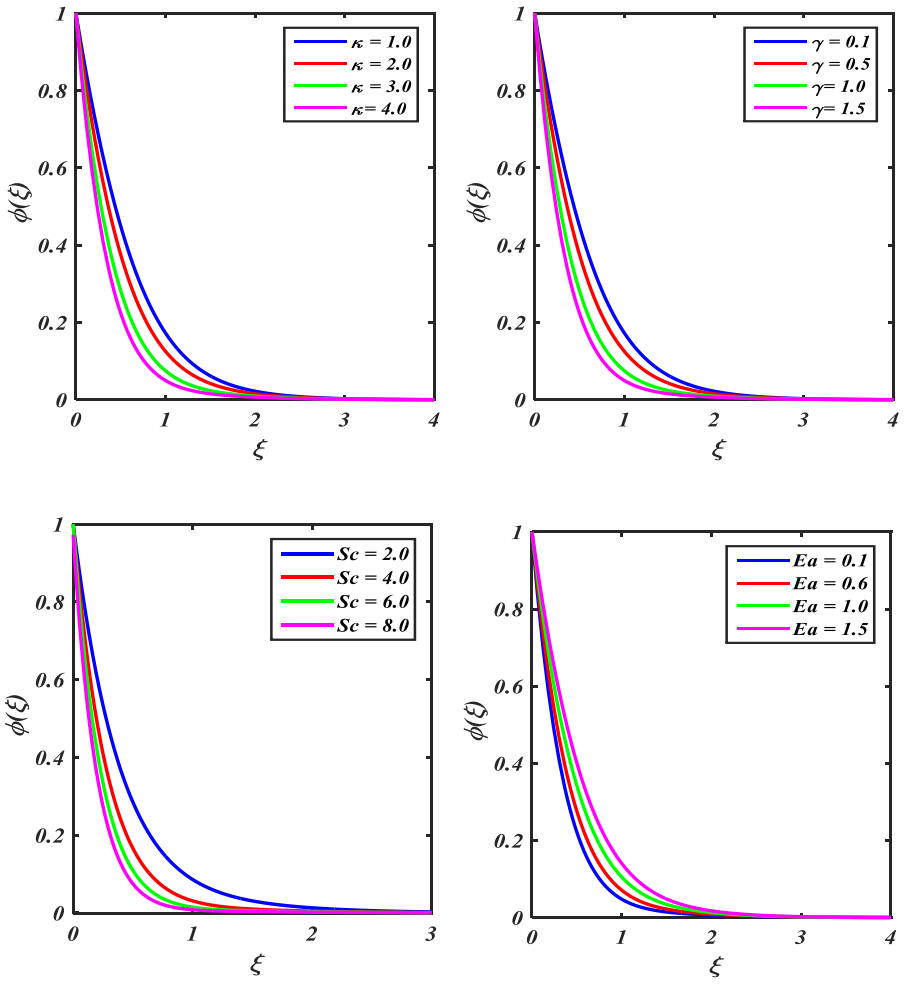

Fig. 7. (a–d) Influence of $\varphi(\xi)$ against (a) κ (b) γ.(c) Sc (d) E_a.

$$\left.\begin{array}{l} P_1 = 0, P_2 = \beta_1 P_3(1-2KP_2), P_4 = \beta_2 P_5(1-2KP_2)+1, P_7 = -Bi(1-P_6), P_8 = 1, P_{10} = 1 \\ P_2 \to 0, P_4 \to 0, P_6 \to 0, P_8 \to 0, P_{10} \to 0. \end{array}\right\} \tag{36}$$

In these numerical simulations, it is necessary to carefully select initial assumptions to ensure that the solution will satisfy the initial conditions. To arrive at a convergent final result, the iterations have been carried out numerous times. When compared to other analytical procedures, these results are very efficient. Typically, the values assigned to the provided parameters are decided upon using the convergence above criteria. Each iteration of the process is carried out based on the value of a newly allocated parameter.

The boundary condition in Eq. (37) is calculated by using of finite value for $\xi_{\max}$ as gives

$$F'(\xi)_{\max} = 0, G(\xi)_{\max} = 0, \theta(\xi)_{\max} = 0, \varphi(\xi)_{\max} = 0, \Upsilon(\xi)_{\max} = 0 \tag{37}$$

The step size is taken $\Delta\xi = 0.001$ and convergent criteria are preferred to obtain a numerical solution.

4. Entropy generation

The entropy minimization [48] on the volumetric rate of Reiner-Rivlinnanofluid is given in Eq. (38).

$$\left.\begin{array}{l} G_s = \dfrac{k}{T_\infty^2}\left(1+\dfrac{16\sigma * T_\infty^3}{3kk*}T_z\right)^2 + \dfrac{1}{T_\infty}\left[\begin{array}{l} 2u_r\tau_{rr} + 2\left(\dfrac{1}{r}v_\varphi + \dfrac{u}{r}\right)\tau_{rr} + 2w_z\tau_{zz} + 2\left(\dfrac{1}{r}u_\varphi + \left(\dfrac{u}{r}\right)_r\right)\tau_{\varphi r} \\ +w_r\tau_{rz} + 1/rw_\varphi\tau_{z\varphi} \end{array}\right] \\ \quad + \dfrac{\mathrm{H}_w}{T_\infty}T_zC_z + \dfrac{\mathrm{H}_w}{C_\infty}(C_z)^2 + \dfrac{\mathrm{H}_w}{N_\infty}(N_z)^2 + \dfrac{\mathrm{H}_w}{T_\infty}(N_zC_z) + \dfrac{\mu u^2}{T_\infty k} + \dfrac{\sigma B_0^2}{T_\infty}u^2. \end{array}\right\} \tag{38}$$

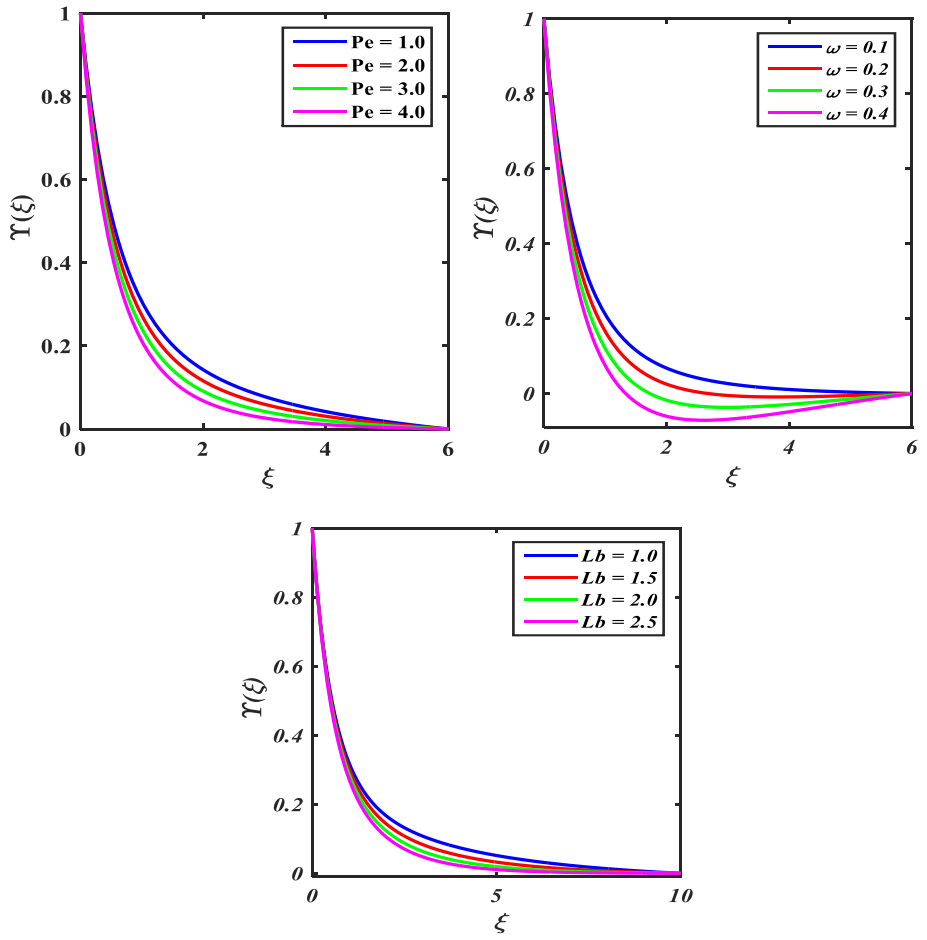

Fig. 8. (a–c) Influence of $\Upsilon(\xi)$ variation in (a) *Pe* (b) ω (c) *Lb*.

The dimensionless entropy generation is developed as

$$N_s = \frac{Gs}{G_0'''} \tag{39}$$

$$N_s = \Omega_a\left(1+\frac{4}{3}Rd\right) + Br\left[\left(\begin{array}{l}\frac{1}{\mathrm{Re}}F'2+\lambda F'3\left\{\frac{16-2\mathrm{Re}}{\mathrm{Re}}\right\}-2\lambda F'F''2\\ -2\lambda F'G'2+MF'\end{array}\right)\right] + \mathrm{X}\theta'\varphi' + \mathrm{X}\frac{\Omega_b}{\Omega_a}\varphi'2 + \mathrm{X}_a\theta'\Upsilon' + \frac{\Omega_c}{\Omega_a}\Upsilon'2 \tag{40}$$

where

$$Br = \frac{\mu\Omega^2}{k(T_0-T_\infty)}, X = \frac{\mathrm{H}_w(C_w-C_\infty)}{k}, X_1 = \frac{\mathrm{H}_w(N_w-N_\infty)}{k}, G_0''' = \frac{k(T_0-T_\infty)}{vT_\infty}.$$

5. Result and discussion

To examine the governing physical parameters, the profiles of $F(\xi)$, $F'(\xi)$, $G(\xi), \varphi(\xi), \theta(\xi), \Upsilon(\xi)$ have been sketchedin Figs. 2–10. Fig. 2(a)-2(d) are portrayed to see the role of the Reiner-Rivlin fluid variables λ ontheaxial velocity $F(\xi)$, the radialvelocity $F'(\xi)$, the tangential $G(\xi)$, the temperature $\theta(\xi)$, andtheconcentration $\varphi(\xi)$ and the motile organism $\Upsilon(\xi)$. Fig. 2(a) exhibits the outcome of the λ over the axial velocity $F(\xi)$. Reducing performance is exhibited in the axial velocity $F(\xi)$ with increasingvaluesof λ. In addition, it has been shown that persuaded the axial motion goes to condense with the wall slip that is far from the disc and has little impact close to the wall areas. Fig. 2(b) displays that the behavior of $F'(\xi)$ falls down when slip is there and uplifts away nearby disk due to the rising values of λ. Moreover, it notices that when λ is high, the absolute maxima in the lower vertical distance also causes the axial flow to

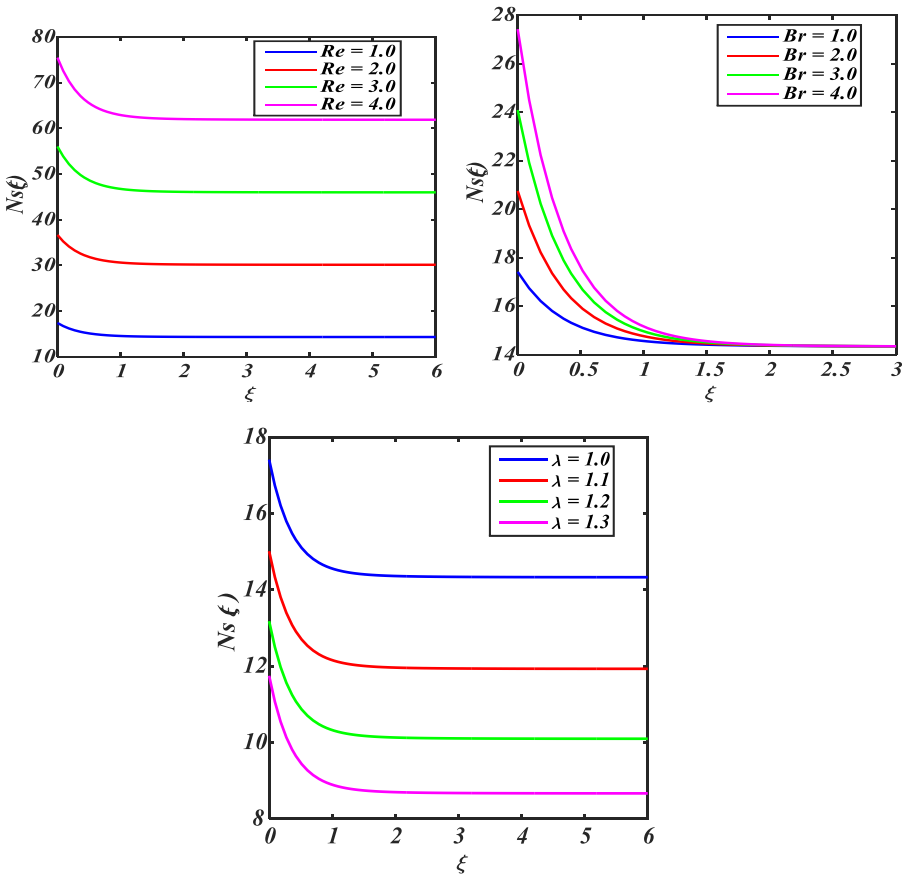

Fig. 9. (a–c) Influence of *Ns* variation in (a) Re (b) *Br* (c) λ.

slow down. As a result, the velocity falls as the values of λ increase. Physically, the less fluid is compressed axially due to increase in the radial fluid expulsion which causes by the viscoelastic processes. It is concluded that the traditional von-Karman issue continues to behave such a centrifugal in the non-Newtonian scenario. However, the consequences become more pronounced when slips are absent. Fig. 2(c) and (d) suggest the increasing behavior of the tangential velocity $G(\xi)$ and temperature distribution $\theta(\xi)$ with λ. Fig. 3 (a)-3(d) observe that the axial $F(\xi)$, the radial $F^{'}(\xi)$, and the tangential $G(\xi)$ velocities and temperature distribution $\theta(\xi)$ are depreciated with the larger value of *M*. Actually, the Lorentz force which develops drag force has the propensity to drop down the flow along the disk surface. While, the opposite trend is recorded in temperature distribution as noticed in Fig. 3(d). The impact of Biot number *Bi* on the temperature profile $\theta(\xi)$ is displayed in Fig. 4(a). The temperature and thermal boundary layer thickness enhanceforan increasing valuesof *Bi*. Here, the enhancement in *Bi* ultimately increasing the heat transport that strikes more heat from the disk. Due to this, the temperature is enhanced. The behavior of *Ec* and *Rd* on the temperature profile $\theta(\xi)$ is plotted in Fig. 4(b)-4(c). These figures suggest that thetemperature augments due to *Ec* and *Rd*. This is because the radiative heat transfer is encouraging for the thermal boundary layer increment. TheInfluence of Pr on the temperature profile is seen in Fig. 4(d). The temperature declinesdueto Pr. As Pr rises, the heat conductivity declines. Physically, a larger PrandtlPrdenotes the poor thermal conductivity, which decays conduction and in turns the thermal boundary layer leading to a drop in fluid temperature. The role of *Nb* on the temperature and the concentration distribution is elaborated in Fig. 5(a)-5(b). Fig. 5(a) shows how the Brownian motion parameter *Nb* responds to the temperature. The temperature increases with the increasing value of *Nb*.Physically, the increased Brownian motion parameter causes nanoparticle motion in the fluid flow to speed up, extending the thickness of the thermal boundary layer and rapidly increasing the temperature of the nanofluid. Fig. 5(b) illustrates how stronger Brownian diffusion causes greater motion, which raises the concentration of the nanoparticles. Thethermophoretic force on the temperature field $\theta(\xi)$ and concentration of nanoparticle $\varphi(\xi)$ are portrayed in Fig. 6(a)-6(b). The temperature field $\theta(\eta)$ is uplifted for larger valuesof *Nt*. However, the concentration $\varphi(\eta)$ displays the depreciationwithan improving values of *Nt* as shown in Fig. 6(b). It is the fact that particles near the hot walls develop the thermophoreticforce, this force amplifies the temperature in the fluid area. Fig. 7(a)-7(d) display the impact of the chemical reaction κ, the temperature relative γ, Schmidt number Sc, and activation energy E_a on the concentration of nanoparticles $\varphi(\xi)$. Fig. 7(a), (b) and 7(c) showthattheconcentration of nanoparticles decline with increasing values of κ,γ, and *Sc*. In contrast, the concentration $\varphi(\eta)$ augments due to the larger values ofactivation energy E_a as shown in Fig. 7(d). Infact E_a diminishes the amend Arrhenius function which result promotes the generative chemical reaction and thus concentration is mounted.

$\beta_1 = 1.0$	$\beta_1 = 1.5$	$\beta_1 = 2.0$
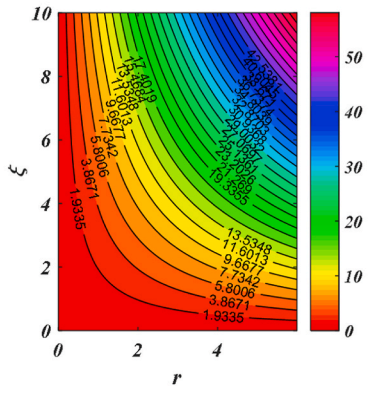	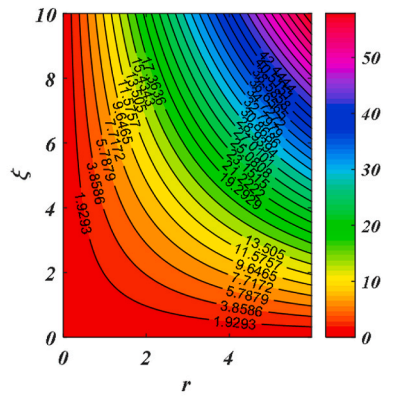	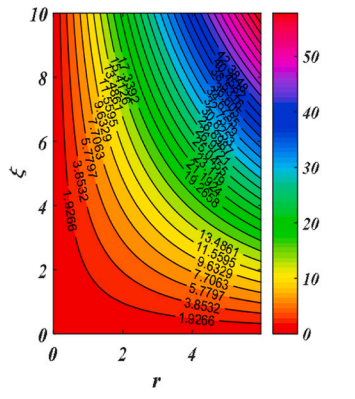
(a)	(b)	(c)
$\beta_2 = 1.0$	$\beta_2 = 2.0$	$\beta_2 = 2.5$
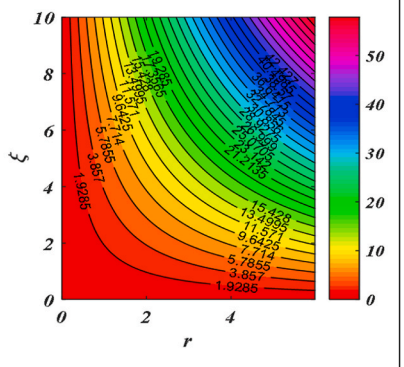	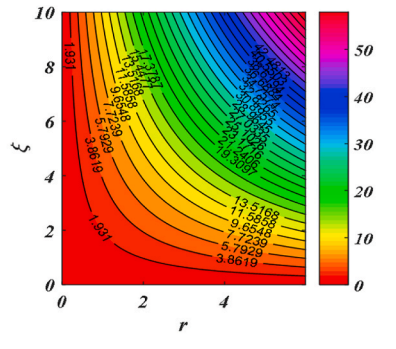	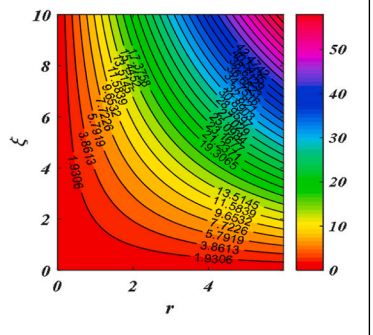
(d)	(e)	(f)
$\lambda = 1.5$	$\lambda = 2.0$	$\lambda = 2.5$
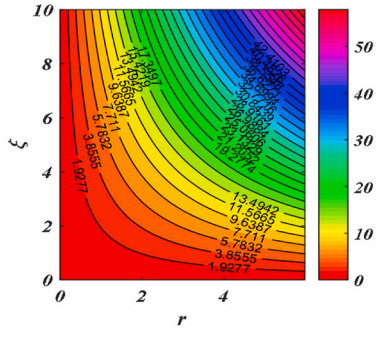	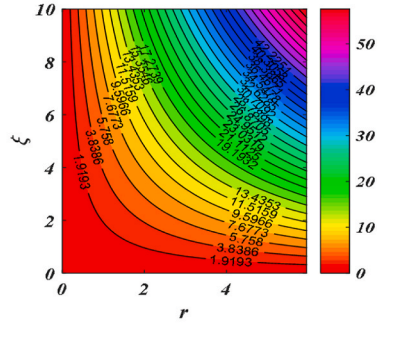	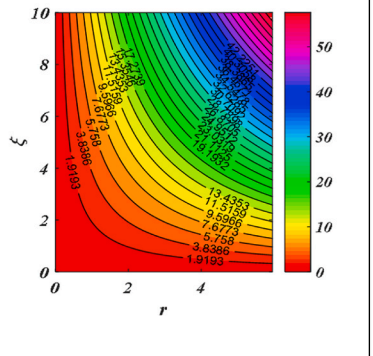
(g)	(h)	(i)

(caption on next page)

Fig. 10. Contour plot for the various values of $\beta_1, \beta_2, \lambda$.

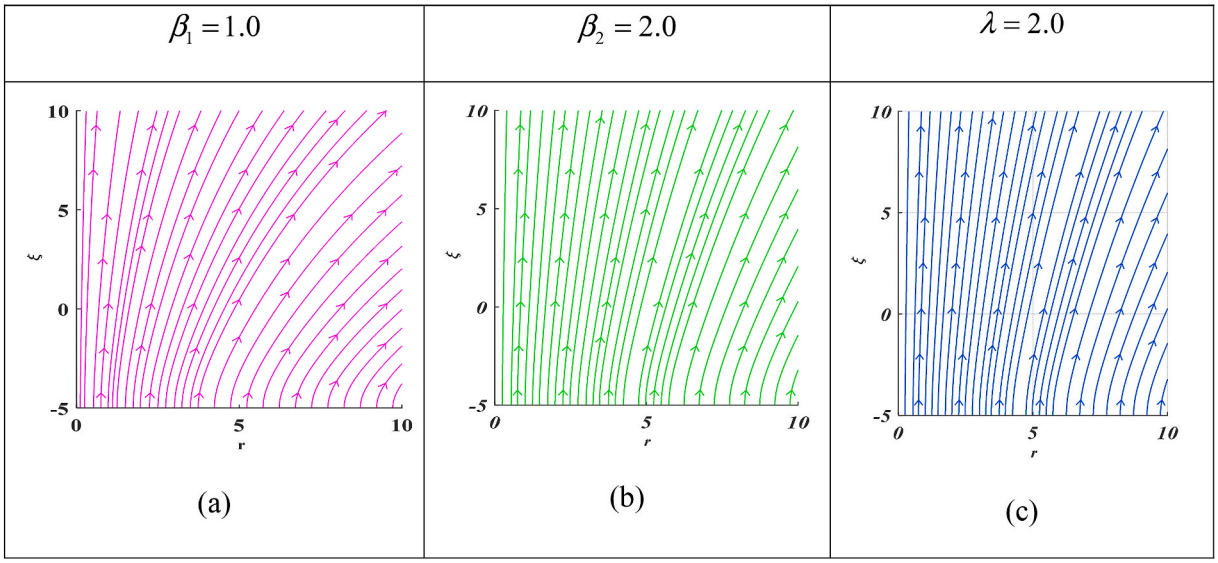

Fig. 11. Streamline for the various values of $\beta_1, \beta_2, \lambda$.

Table-1
Comparing of $-F''(0)$ with present results when all other parameters are zero.

β_1	β_2	Abdal et al. [48]	Present result
0	0	0.5102326	0.5102
1	1	0.1279236	0.1279
5	5	0.0185885	0.0185
10	10	0.0068125	0.0068
20	20	0.0023614	0.0002
40	40	0.0007899	0.0007

Table-2
Comparing of $-G'(0)$ and present results when all other parameters are zero.

β_1	β_2	Abdal et al. [48]	Present result
0	0	0.6159220	0.6159
1	1	0.3949275	0.3949
5	5	0.1433882	0.1433
10	10	0.0810300	0.0810
20	20	0.0437883	0.0437
40	40	0.0229952	0.0229

Fig. 8(a) shows how the bioconvectionPeclet number *Pe* affects the motile density profile $\Upsilon(\xi)$. The graph shows that an increase in *Pe* causes a condensing of microbe density. Since *Pe* is described to the physical indicator of the relation power of motile microorganisms' directed and zigzag swimming. As a result, the larger values of *Pe* indicates that the bacteria are moving in reverse more frequently, which reduces the concentration profile. In Fig. 8(b)-8(c), the same trend is seen for *Lb* and ω as depicted in Fig. 8(b)–8(c). Fig. 9(a)–(c) illustrate the significance of the volumetric entropy for various values ofRe, Br and λ. Entropy increases as Br and Re increase. The viscous dissipation produces a lower transfer rate at high levels of Br, which increases the entropy formation. When Br = 0, only heat transfer irreversibility remains and viscous dissipative irreversibility vanish. In Fig. 9(b), the impact of Re on the entropy is seen. The significant of mobility of the fluid molecules is noticed for higher Reynolds number estimations as a result, anincreasing the pace of the entropy. Fig. 9(c)shows a drop in the entropy at the larger values of the Reiner-Rivlinparameter λ. In the end, the contour plot and stream lineare presented in Fig.. 10(a–i) and 11 (a-c)a–i a-cFig. 10(a–i) and 11 (a-c)Fig. 10(a–i) and 11 (a-c)Fig. 10(a–i) and 11 (a-c) for numerous values $\beta_1, \beta_2, \lambda$.

The current numerical is validated with previous literature by Abdal et al. [49] and found an outstanding achievement as depicted in Tables 1 and 2. Table 3 displays the current numerical findings for various wall roughness levels and Reiner-Rivlin parameters for

Table-3
Computational values of $F(\infty)$, $F''(0)$, $G^{'}(0)$ wall stressalong with skin frictionagainst numerous values M, λ, β_1, β_2.

M	λ	β_1	β_2	F(∞)	F″(0)	G′(0)	$-\sqrt{(F''(0))^2+(G'(0))^2}$
0.5	1	1.0	1.0	0.2886	0.0315	0.4349	0.1046
		1.3		0.3536	0.0275	0.4592	0.1058
		1.5		0.4047	0.0254	0.4608	0.1065
		1.8		0.4186	0.0228	0.4627	0.1073
			1.1	0.4447	0.0183	0.3876	0.0753
			1.5	0.4939	0.0174	0.3724	0.0695
			1.6	0.5025	0.0165	0.3585	0.0644
			1.7	0.6229	0.0157	0.3455	0.0598
	1.3			0.6720	0.0149	0.3404	0.0580
	1.4			0.7234	0.0134	0.3382	0.0572
	1.5			0.7521	0.0127	0.3231	0.0555
	1.6			0.8132	0.0121	0.3132	0.0538
	1.7			0.8537	0.0119	0.3041	0.0521
0.1				0.8756	0.0465	0.3432	0.0597
0.2				0.9063	0.0321	0.3353	0.0567
0.3				0.9176	0.0208	0.3112	0.0553
0.4				0.9182	0.0121	0.0291	0.0510

Table-4
Computational values of heat transfer rate M, λ, Nt, Nb, Rd, Ec, κ, E_a.

M	λ	Nt	Nb	Rd	Ec	κ	E_a	$-\theta^{'}(0)$
0.5	0.2	0.4	0.4	0.2	0.2	1	1	0.6571
1.0								0.5658
1.5								0.4886
1	0.1							0.5313
	0.3							0.5658
	0.5							0.5953
	0.3	0.3						0.6010
		0.6						0.4995
		0.9						0.4099
		0.4	0.3					0.5658
			0.6					0.5658
			0.9					0.5658
			0.4	0				0.5059
				0.1				0.5365
				0.2				0.5658
					0			0.7675
					0.2			0.5658
					0.4			0.3630
						1		0.5658
						2		0.5520
						3		0.5427
							1	0.5658
							2	0.5748
							3	0.5790
								0.6379
								0.7719
								0.9028

velocity $F(\infty)$, radial $F''(0)$ and azimuthal wall stress $G^{'}(0)$, as well as the skin friction. Entrainment velocity $F(\infty)$ may be used to calculate the von-Karman problem's volumetric flow rate. The radial wall stress $F''(0)$, azimuthal wall stress $G^{'}(0)$ and wall friction are calculated for various values of β_1, β_2, and λ. As the values of β_1, β_2, and λ increase, it is found that the values of radial and azimuthal wall stresses decrease. Table 4 displays the rate of heat flux for numerous values of Rd,Nb,Nt. It is seen that for the large values of Rd,Nb, Nt, the Nusselt number decreases and the opposing effects are seen for E_a,κ,γ. Table 5 displays the rate of mass flux for numerous values of γ,E_a,Sc. It is seen that for the large values of γ,E_a,Sc, the Sherwood number increases. Table 6 views numerous estimations in the local density profile for different values of Lb, Pe, ω. It is observed that for large estimates of Lb, Pe, ω, the local density number of micro-organisms increases.

6. Conclusion

The current article aims to examine the flow of Reiner-Rivlinnanofluidin the presence of microorganisms due to rotating disk with viscous dissipation and Arrhenius activation energy. The flow is also accomplished by the multiple slip effect, convective condition and

Table-5
Computational values of Mass transfer rate Nt, Nb, Rd, Sc, κ, E_a, γ.

Nt	Nb	Rd	Sc	κ	E_a	γ	$-\varphi'(0)$
0.4	0.4	0.2	1.0	1.0	1.0	0.5	0.9781
			2.0				1.2823
			3.0				1.4960
			4.0				1.5313
				2.0			2.1354
				2.5			2.3221
0.3				3.0			2.4913
0.6				3.5			2.6473
0.9					1.5		2.7200
0.4	0.3				2.0		2.7953
	0.6				2.5		2.8733
	0.9				3.0		2.9542
	0.4	0				1.0	3.0380
		0.1				1.5	3.1249
		0.2				2.0	3.2150
			0			2.5	3.3084
			0.2				3.4054
			0.4				3.5059

Table-6
Computational values of Motile transfer rate Nb, Nt, Sc, κ, E_a, Pe , ω, Lb.

Nb	Nt	Sc	κ	E_a	Pe	ω	Lb	$-\Upsilon'(0)$
0.4	0.4	1.0	1.0	1.0	0.5	0.5	0.5	1.3430
		2.0						1.3746
		3.0						1.4060
		4.0						1.4194
			2.0		1.0			1.4381
			2.5		1.3		1.0	1.4562
0.3			3.0		1.6			1.4737
0.6			3.5		1.9			1.4987
0.9				1.5				1.5772
0.4	0.3			2.0				1.6808
	0.6			2.5				1.7841
	0.9			3.0				1.8875
	0.4				1.0			1.9910
					1.5			2.0944
					2.0			2.1979
		0			2.5			2.3013
		0.2					1.0	2.4048
		0.4						2.5083

thermal radiation. The problem is solve by using bvp4c technique. The Key observations are as follows.

- A higher value of the Reiner-Rivlin parameter λ results in diminishing the axial and radial velocities. However, the azimuthal velocity and temperature profile exhibit a negative correlation. Physically, this is due to the enhanced cross-viscosity, which improves non-Newtonian behavior.
- The magnetic field displays deprecating behavior against the radial and tangential velocities.
- For increasing estimation of the Eckert number, the fluid temperature is raised.
- The activation energy parameters and chemical reactions have conflicting effects on the concentration profile.
- For higherPeclet and bioconvective Lewis numbers, the motile density profile decreases.
- Contradictory trends regarding volumetric entropy generation may be seen in the Brinkman and Reiner –Rivlin parameters.

7. Future direction

With the help of these computational efforts, we have been able to successfully elucidate the MHD flow of multiple slip effect on Reiner-Rivilinnanofluid as well as the activation energy effects over a rotating disk. This study has the potential to be expanded to include the Stagnation point flow, mixed convection flow, Darcy Forchheimer flow and generalized fluids models.

Author contribution statement

1) conceived and designed the experiments;

2) performed the experiments;
3) analyzed and interpreted the data;
4) contributed reagents, materials, analysis tools or data;
5) wrote the paper.

Funding statement

This research was funded by National Science, Research and Innovation Fund (NSRF), King Mongkut's University of Technology North Bangkok with Contract no. KMUTNB-FF-66-36 and the Center of Excellence in Theoretical and Computational Science (TaCS-CoE), KMUTT.

Data availability statement

Data will be made available on request.

Declaration of interest's statement

The authors declare no competing interests.

References

[1] S.U.S. Choi, J. Eastman, Enhancing Thermal Conductivity of Fluids with Nanoparticles, vol. 231, ASME-Publications-Fed, 2001, pp. 718–720.
[2] J. Buongiorno, Convective transport in nanofluids, J. Heat Tran. 128 (2006) 240–250.
[3] R.K. Tiwari, M.K. Das, Heat transfer augmentation in a two-sided lid-driven differentially heated square cavity utilizing nanofluids, Int. J. Heat Mass Tran. 50 (2007) 2002–2018.
[4] J.A. Khan, M. Mustafa, T. Hayat, M.A. Farooq, A. Alsaedi, S.J. Liao, On model for three-dimensional flow of nanofluid: an application to solar energy, J. Mol. Liq. 194 (2014) 41–47.
[5] S. Mansur, A. Ishak, Three-dimensional Flow and Heat Transfer of a Nanofluid Past a Permeable Stretching Sheet with a Convective Boundary Condition, AIP Conference Proc. AIP, 2014, pp. 906–912.
[6] M. Sheikholeslami, H.M. Hatami, D.D. Ganji, Nanofluid flow and heat transfer in a rotating system in the presence of a magnetic field, J. Mol. Liq. 190 (2014) 112–120.
[7] M. Alghamdi, Significance of Arrhenius activation energy and binary chemical reaction in mixed convection flow of nanofluid due to a rotating disk, Coat 10 (1) (2020) 86.
[8] M. Jawad, Z. Shah, S. Islam, J. Majdoubi, I. Tlili, W. Khan, I. Khan, Impact of nonlinear thermal radiation and the viscous dissipation effect on the unsteady three-dimensional rotating flow of single-wall carbon nanotubes with aqueous suspensions, Symmetry 11 (2019) 207.
[9] Z. Shah, A. Dawar, P. Kuman, W. Khan, S. Islam, Impact of nonlinear thermal radiation on MHD nanofluid thin film flow over a horizontally rotating disk, Appl. Sci. 9 (2019) 1533.
[10] S.M. Raza Shah Naqvi, H.M. Kim, T. Muhammad, F. Mallawi, M.Z. Ullah, Numerical study for slip flow of Reiner-Rivlinnanofluid due to a rotating disk, Int. com. Heat Mass Trans. 116 (2022), 104643.
[11] F. Ali, A. Zaib, Unsteady flow of an Eyring-Powell nanofluid near stagnation point past a convectively heated stretching, sheet, Arab J. Basic Appl. Sci. 26 (2019) 215–224.
[12] V. Puneeth, F. Ali, Khan, M.S. Anwar, N.A. Ahmed, Theoretical Analysis of the Thermal Characteristics of Ree–Eyringnanofluid Flowing Past a Stretching Sheet Due to Bioconvection, Biomass Conv. Bioref., 2022, https://doi.org/10.1007/s13399-022-02985-1.
[13] T. Muhammad, A. Alsaedi, S.A. Shehzad, T. Hayat, A revised model for Darcy-Forchheimer flow of Maxwell nanofluid subject to convective boundary condition, Chin. J. Phys. 55 (2017) 963–976.
[14] T. Hayat, T. Muhammad, S.A. Shehzad, A. Alsaedi, Onthemagnetohydrodynamic flow of nanofluid due to a rotating disk with slip effect: a numerical study, Comput. Methods Appl. Mech. Eng. 315 (2017) 467–477.
[15] T.V. Karman, Überlaminare und turbulenteReibung, Z. Angew. Math. Mech. 4 (1921) 233–252.
[16] W. Cochran, The flow due to a rotating disc, Math. Proc. Camb. Phil. Soc. 30 (3) (1934) 365–375. Cambridge University Press.
[17] K.P.K. Millsaps, Heat transfer by laminar flow from a rotating plate, J. Aeronaut. Sci. 19 (1952) 120–126.
[18] J. Ackroyd, On the steady flow produced by a rotating disc with either surface suction or injection, J. Eng. Math. 12 (1978) 207–220.
[19] G.K. Batchelor, Note on a class of solutions of the Navier-Stokes equations representing steady rotationally-symmetric flow, Quart. J. Mech. Appl. Math. 4 (1951) 29–41.
[20] V.U. Bödewadt, Die drehströmungüberfestemgrunde, Z. Angew. Math. Mech. 20 (1940) 241–253.
[21] P. Zandbergen, D. Dijkstra, Von Kármán swirling flows, Annu. Rev. Fluid Mech. 19 (1987) 465–491.
[22] P.D. Ariel, Computation of flow of a second grade fluid near a rotating disk, Int. J. Eng. Sci. 35 (1997) 1335–1357.
[23] S.S. Chawla, P.K. Srivastava, A.S. Gupta, Rotationally symmetric flow over a rotating disk, Int. J. Non Lin. Mech. 44 (2009) 717–726.
[24] M. Miklavčič, C. Wang, The flow due to a rough rotating disk, ZAMP 55 (2004) 235–246.
[25] M. Turkyilmazoglu, Three dimensional MHD stagnation flow due to a stretchable rotating disk, Int. J. Heat Mass Tran. 55 (2012) 6959–6965.
[26] M. Turkyilmazoglu, Fluid flow and heat transfer over a rotating and vertically moving disk, Phys. Fluids 30 (2018), 063605.
[27] M. Turkyilmazoglu, Direct contact melting due to a permeable rotating disk, Phys. Fluids 31 (2019), 023603.
[28] O.A. Bég, M.J. Uddin, T.A. Bég, A. Kader, M.D. Shamsuddin, M. Babaie, Numerical study of self-similar natural convection mass transfer from a rotating cone in anisotropic porous media with Stefan blowing and Naviershp, Indian J. Phys. 94 (2020) 863–877.
[29] O.A. Bég, M.N. Kabir, M.J. Uddin, I.M. Ismail, Y.M. Alginahi, Numerical investigation of Von Karman swirling bioconvectivenanofluid transport from a rotating disk in a porous medium with Stefan blowing and anisotropic slip effects, Proc. Inst. Mech. Eng. *Part C.* 235 (19) (2021) 3933–3951.
[30] N.A. Latiff, M.J. Uddin, A. I. Md Ismail, Stefan blowing effect on bioconvective flow of nanofluid over a solid rotating stretchable disk, Propuls. Power Res. 5 (4) (2016) 267–278.
[31] T.Z. Fatema, M.J. Uddin, M.F. Basir, A.I. Md Ismail, Magnetohydrodynamic bio-nano-convective slip flow with stefan blowing effects over a rotating disc, Proc. Inst. Mech. Eng. N: J. Nanomater. Nanoeng. Nanosyst. 234 (3–4) (2020) 83–97.
[32] T.Z. Fatema, M.J. Uddin, M.F. Basir, A.I. Md Ismail, Magnetohydrodynamic bio-NanoconvectiveNaiver slip flow of micropolar fluid in a stretchable horizontal channel, Heat Tran. Res. 48 (8) (2019) 3636–3656.
[33] M. J Uddin, M.N. Kabir, Y. Alginahi, O.A. Bég, Numerical solution of bio-nano-convection transport from a horizontal plate with blowing and multiple slip effects, Proc. Inst. Mech. Eng. C: J. Mech. 233 (19–20) (2019) 6910–6927.

[34] P. Biswas, S.M. Arifuzzaman, Md M. Rahman, M.S. Khan, Effects of periodic magnetic field on 2D transient optically dense gray nanofluid over a vertical plate: a computational EFDM study with SCA, J.Nanofluids 7 (1) (2018) 82–91.
[35] S.M. Arifuzzaman, M. Mehedi, A. Al-Mamun, P. Biswas, Md Islam, Md Khan, MagnetohydrodynamicMicropolar fluid flow in presence of nanoparticles through porous plate: a numerical study, Int. J. Heat Technol. 36 (3) (2018) 936–948.
[36] M. Reiner, A mathematical theory of dilatancy, Am. J. Math. 67 (3) (1945) 350–362.
[37] R. Rivlin, Hydrodynamics of non-Newtonian fluids, Nature 160 (4070) (1947) 611.
[38] L. Elliott, Elastico-viscous flow near a rotating disk, Phys. Fluids 14 (1971) 1086–1090.
[39] P.D. Ariel, On the flow of an elastico-viscous fluid near a rotating disk, J. Comput. Appl. Math. 154 (2003) 1–25.
[40] H.I. Anderssen, E.D. Korte, MHD flow of a power-law fluid over a rotating disk European, J.Mech-B/Fluids 21 (2002) 317–324.
[41] E. Osalusi, J. Side, R. Harris, B. Johnston, On the effectiveness of viscous dissipation and Joule heating on steady MHD flow and heat transfer of a Bingham fluid over a porous rotating disk in the presence of Hall and ion-slip currents, Int. Commun. Heat Mass Tran. 34 (2007) 1030–1040.
[42] H.A. Attia, Rotating disk flow and heat transfer through a porous medium of a non-Newtonian fluid with suction and injection, Comm. Nonlinear Sci. No.Simul. 13 (2008) 1571–1580.
[43] B. Sahoo, Effects of partial slip, viscous dissipation and Joule heating on von Kármán flow and heat transfer of an electrically conducting non-Newtonian fluid, Comm. Nonlinear Sci. Numer. Simul. 14 (2009) 2982–2998.
[44] A. Ahmadpour, K. Sadeghy, Swirling flow of Bingham fluids above a rotating disk: an exact solution, J. Newtonian Fluid Mech. 197 (2013) 41–47.
[45] M. Imtiaz, F. Mabood, T. Hayat, A. Alsaedi, Homogeneous-heterogeneous reactions in MHD radiative flow of second grade fluid due to a curved stretching surface, Int. J. Heat Mass Tran. 145 (2019), 118781.
[46] B. Sahoo, I.V. Shevchuk, Heat transfer due to revolving flow of Reiner-Rivlin fluid over a stretchable surface, Therm. Sci. Eng. Prog. 10 (2019) 327–336.
[47] Y.P. Lv, H. Gul, M. Ramzan, J.D. Chung, M. Bilal, Bioconvective Reiner–Rivlinnanofluid flow over a rotating disk with Cattaneo–Christov flow heat flux and entropy generation analysis, Sci. Rep. 11 (2021), 15859.
[48] S. Abdal, A. Mariam, B. Ali, S. Younas, Liaqat Ali, D. Habib, Implications of bioconvection and activation energy on Reiner–Rivlinnanofluid transportation over a disk in rotation with partial slip, Chin. J. Phys. 73 (2021) 672–683.